# THE EFFECT OF NEWLY ERUPTING FLUX ON THE POLAR CORONAL HOLES

N. R. SHEELEY, JR., Y.-M. WANG[1], and J. W. HARVEY[2]

*E.O. Hulburt Center for Space Research, Naval Research Laboratory, Washington, DC 20375-5000, U.S.A.*

(Received 21 July, 1988)

**Abstract.** He I 10830 Å images show that early in sunspot cycles 21 and 22, large bipolar magnetic regions strongly affected the boundaries of the nearby polar coronal holes. East of each eruption, the hole boundary immediately contracted poleward, leaving a band of enhanced helium network. West of the eruption, the boundary remained diffuse and gradually expanded equatorward into the leading, like-polarity part of the bipolar magnetic region. Comparisons between these observations and simulations based on a current-free coronal model suggest that:

(1) The Sun's polar magnetic fields are confined to relatively small caps of high average field strength, apparently by a poleward meridional flow.

(2) The enhanced helium network at high latitude marks the location of relatively strong polar fields that have become linked to the newly erupted bipolar region in that hemisphere.

(3) The distortion of the polar-hole boundary is accompanied by a corresponding distortion of the equatorial neutral sheet in the outer corona, in which the amount of warping depends on the magnitude of the erupted flux relative to the strength of the Sun's polar magnetic fields.

## 1. Introduction

It is well known that solar images obtained in the lines of He I and He II show characteristics of both the chromosphere and the corona. On the one hand, they show the chromospheric network, either bright against a darker background as in the He I 584 Å and He II 304 Å emission lines (Tousey, 1967, 1971; Tousey *et al.*, 1973), or dark against a brighter background as in the He I 5876 Å and 10830 Å absorption lines (D'Azambuja and D'Azambuja, 1938; Zirin and Howard, 1966; Harvey and Hall, 1971; Giovanelli, Hall, and Harvey, 1972; Chapman, 1972; Harvey *et al.*, 1975; Harvey and Sheeley, 1977). On the other hand, these images show large-scale spatial variations of intensity which are strongly correlated with patterns of coronal intensity: network weakenings mark the location of coronal holes, where magnetic field lines are open (Bohlin and Rubenstein, 1975; Harvey and Sheeley, 1979). Network enhancements mark closed-field regions of relatively high average field strength, such as bipolar magnetic regions and their remnants, ephemeral magnetic regions (Harvey, 1984, 1985), and the two-ribbon components of some flares (Harvey *et al.*, 1980; Harvey, Sheeley, and Harvey, 1986; Sheeley and Harvey, 1981).

[1] Applied Research Corporation, Landover, MD 20785, U.S.A.

[2] National Solar Observatory*, Tucson, AZ 85726, U.S.A.

* Operated by the Association of Universities for Research in Astronomy, Inc., under contract with the National Science Foundation.

*Solar Physics* **119** (1989) 323–340.

The purpose of this paper is to call attention to network enhancements that occur along the edges of the polar coronal holes immediately after sunspot minimum. In Section 2, we illustrate that these enhancements accompany the eruption of the first large high-latitude bipolar magnetic regions of the new sunspot cycle. In Section 3, we show that these eruptions must have encountered relatively concentrated polar fields whose strengths decrease rapidly equatorward of about 60° latitude. In Section 4, we compare the helium observations with current-free magnetic field calculations, and find that the enhanced helium network occurs where relatively strong fields at high latitude become connected to newly erupted bipolar magnetic regions. Finally, in Section 5, we briefly discuss the implications of these results.

## 2. The Observations

We start by examining observations obtained early in sunspot cycle 22, when the polar fields were still strong and large amounts of flux were beginning to erupt at high latitudes. These conditions are illustrated by the sequence of photospheric magnetograms and He I 10830 Å images in Figure 1. Obtained during May 14–24, 1987, these images show remarkably different conditions in the Sun's northern and southern hemispheres. On May 14, the boundary of the north polar coronal hole is poorly visible around N 50–60° latitude, whereas the boundary of the south polar hole is clearly defined by a band of enhanced network at S 65–75°, depending on longitude. Comparison with the corresponding magnetogram reveals that the enhanced network occurs in the positive (white) polarity at the edge of the south polar hole, and is distinct from the enhanced network of negative (black) polarity expanding poleward from the active region near 35° south latitude.

As time passes during May 14–24, the helium enhancements in the southern hemisphere rotate around the west limb, leaving a south polar coronal hole whose boundary at about S 60° latitude is as poorly defined as the one in the northern hemisphere on May 14. Such low-contrast boundaries are characteristic of the coronal holes observed during extended intervals of low sunspot activity near sunspot minimum.

A similar helium enhancement is visible along the edge of the north polar hole during May 18–24, as solar rotation carries a large new bipolar magnetic region across the solar disk. Again, the enhanced network at the edge of the polar hole has the same polarity as the hole itself, in this case negative (black), and is separated from the enhanced network and newly expanding fields of the bipolar region by about 10°. Although not shown here, neither the active region nor the band of enhanced network were present two weeks earlier at the previous west-limb passage of this longitude. Indeed, the enhancement has filled in a portion of the north polar coronal hole up to 65–70° latitude trailing eastward of the active region. However, west of the active region, the polar-hole boundary retains its low contrast and relatively lower latitude. During the next few solar rotations, this polar-hole lobe expanded southward into the leading, like-polarity part of the aging bipolar magnetic region.

Such deformations of the polar-hole boundaries during the rising phase of the sunspot

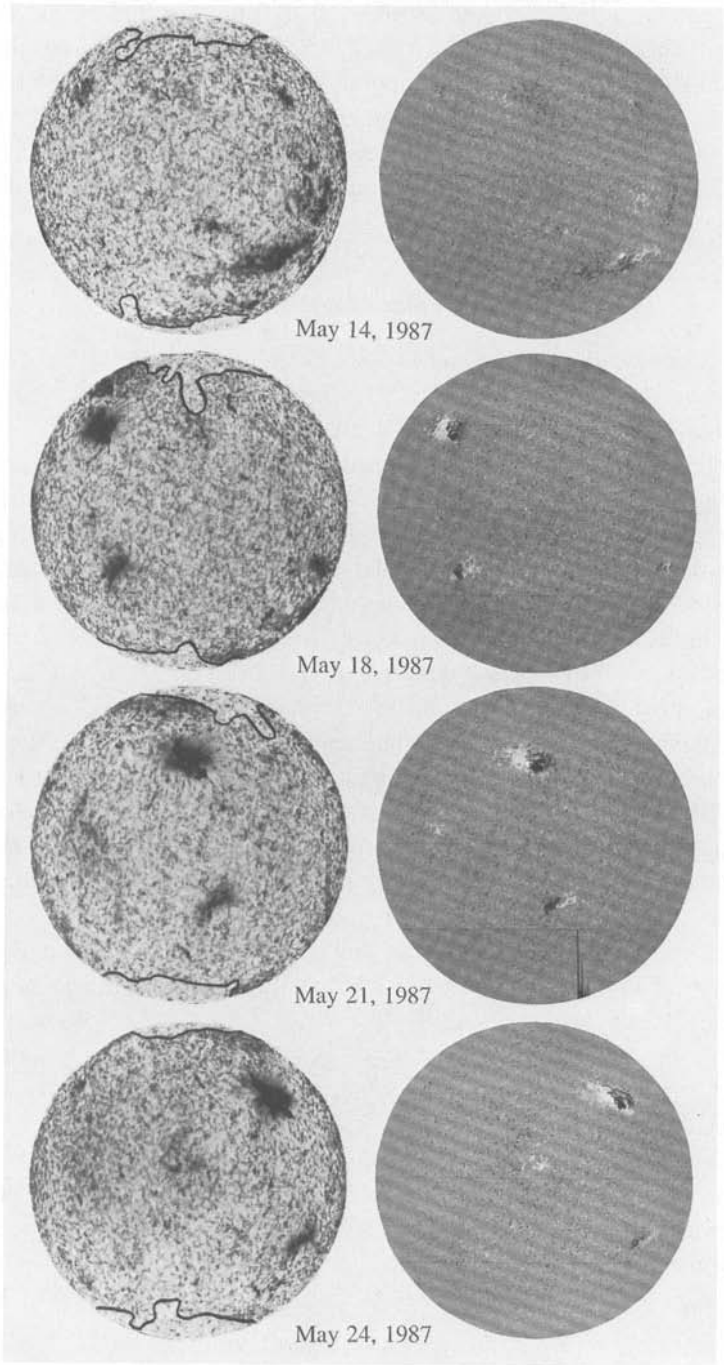


Fig. 1. He I 10830 Å images (left) and corresponding Fe I 8688 Å photospheric magnetograms (right) during the interval May 14–24, 1987. The boundaries of the polar coronal holes are greatly enhanced (*darkened*) adjacent to large regions of newly erupted flux, but they are not enhanced in the quiet hemisphere. In the magnetograms, lighter-than-average features refer to positive line-of-sight polarity and darker features refer to negative polarity.

cycle were predicted by Bohlin and Sheeley (1978) from their analysis of Skylab He II 304 Å images obtained in 1973–1974. Although we subsequently observed them on He I 10830 Å images in 1977 at the beginning of sunspot cycle 21 (Sheeley and Harvey, 1978), we paid little attention to the enhanced network at the edge of the contracted portion of the polar hole. In Section 4, we shall find that this enhancement marks the location of polar flux that has become connected to the opposite pole of the newly erupted bipolar magnetic region.

## 3. The Polar Magnetic Fields

In Section 2, we saw that the boundaries of the polar holes occurred around 60° latitude at times of very low sunspot activity. This result is consistent with measurements obtained from wideband X-ray and XUV images (Broussard *et al.*, 1978), He II 304 Å images (Bohlin, 1977), and He I 10830 Å images (Sheeley, 1980) obtained near previous sunspot minima. Next, we shall see that this result places a severe constraint on the latitude-dependence of the polar magnetic fields.

In order to relate the size of the polar holes to the latitude-dependence of the photospheric flux distribution, we must assume a model for the outward extension of the magnetic field. We begin with the current-free extension described by Schatten, Wilcox, and Ness (1969) and Altschuler and Newkirk (1969). Here, the radial component is required to match the photospheric flux distribution at $r = R$, and open flux is achieved by forcing the non-radial components to vanish at a spherical source surface at $r = R_s$. Following Altschuler and Newkirk (1969) and Hoeksema (1984), we shall take $R_s = 2.5R$, as best fitting the observations. Beyond this source surface, we assume that the field extends radially into the heliosphere where volume currents must therefore exist. Coronal holes are then determined by finding the photospheric footpoints of open field lines.

In this model, all of the source-surface flux of a given polarity must originate within the boundary of the corresponding polar coronal hole. Calling the colatitude of this boundary $\theta_c$ we can then write

$$2\pi R^2 \int_0^{\theta_c} B_r(R, \theta) \sin\theta \, d\theta = 2\pi R_s^2 \int_0^{\pi/2} B_r(R_s, \theta) \sin\theta \, d\theta, \tag{1}$$

where $B_r(R, \theta)$ and $B_r(R_s, \theta)$ are the radial components of the field at the photosphere and at the source surface, respectively. Let us suppose that the photospheric component has the form

$$B_r(R, \theta) = \left(\frac{\Phi_0}{\pi R^2}\right)\left(\frac{n+1}{2}\right)\cos^n\theta =$$

$$= \left(\frac{\Phi_0}{\pi R^2}\right)\left(\frac{n+1}{2}\right)\sum_{l=1}^{n} a_l(n) P_l(\cos\theta), \tag{2a}$$

where $\Phi_0$ is the total amount of photospheric flux of each polarity, and $n$ is an odd integer which indicates how rapidly the field strength decreases away from the poles; also, $l$ is an odd integer, and the coefficients $a_l(n)$ in the series of Legendre polynomials $P_l$ are given by

$$a_l(n) = (2l + 1) \int_0^1 x^n P_l(x)\, dx\,. \tag{2b}$$

Then, the corresponding source-surface field $B_r(R_s, \theta)$ becomes

$$B_r(R_s, \theta) = \left(\frac{\Phi_0}{\pi R^2}\right) \left(\frac{n+1}{2}\right) \sum_{l=1}^{n} c_l(R_s) a_l(n) P_l(\cos\theta)\,, \tag{3a}$$

where the coefficients $c_l(R_s)$ are given by

$$c_l(R_s) = \frac{(2l+1)\varepsilon^{l+2}}{l+1+l\varepsilon^{2l+1}}\,, \tag{3b}$$

and $\varepsilon = R/R_s = 0.4$ (cf. Wang *et al.*, 1988).

Substituting the field components (2a) and (3a) into the open-flux equation (1), and dividing through by the total flux $\Phi_0$, we find that the polar cap angle $\theta_c$ depends on the index $n$ as follows:

$$1 - \cos^{n+1}\theta_c = \left(\frac{R_s}{R}\right)^2 (n+1) \sum_{l=1}^{n} c_l(R_s) a_l(n) \int_0^1 P_l(x)\, dx\,. \tag{4}$$

Also, this procedure gives a convenient relation between the polar-cap half-angle $\theta_c$ and the fraction $f$ of photospheric flux that is contained within the polar coronal holes:

$$f = 1 - \cos^{n+1}\theta_c\,. \tag{5}$$

After some algebra, the integrals in Equations (4) and (2b) can be expressed as

$$\int_0^1 P_l(x)\, dx = \frac{P_{l-1}(0)}{l+1} = (-1)^{[(l-1)/2]} \left(\frac{1}{l+1}\right) \left[\frac{1}{2}\,\frac{3}{4}\,\frac{5}{6} \cdots \left(\frac{l-2}{l-1}\right)\right], \tag{6a}$$

$$\int_0^1 x^n P_l(x)\, dx = \frac{1}{2}\, \frac{\left(\frac{n-1}{2}\right)!}{\left(\frac{n-l}{2}\right)!}\, \frac{\Gamma\left(1+\frac{n}{2}\right)}{\Gamma\left(1+\frac{n}{2}+\frac{l+1}{2}\right)} =$$

$$= \left(\frac{1}{n+2}\right) \left[\left(\frac{n-1}{n+l-1}\right) \left(\frac{n-3}{n+l-1}\right) \left(\frac{n-5}{n+l-3}\right) \cdots \right.$$

$$\left. \cdots \left(\frac{n-l+2}{n+4}\right)\right]. \tag{6b}$$

Using these expressions, we can easily evaluate $f$ and $\theta_c$ as a function of $n$.

The result is shown in the first three columns of Table I. We see that a dipole field ($n = 1$) gives a polar-cap half-angle $\theta_c = 49.7°$, which is much larger than the observed value of 30°. The best fit is obtained for $n$ in the range 7–9, consistent with the polar magnetic field measurements of Svalgaard, Duvall, and Scherrer (1978), who derived $n = 8$. Table I also indicates that relatively more flux is open when it is concentrated toward the poles; in particular, $f = 74\%$ for an $n = 9$ distribution compared to $f = 58\%$ for a dipole field with $n = 1$.

For completeness, we note that smaller values of $\theta_c$ could be obtained by placing the source surface farther from the Sun. However, as Nash, Sheeley, and Wang (1988) have pointed out, it would be necessary to adopt the unrealistically large value of $R_s/R = 6.0$ in order to obtain $\theta_c = 30°$ with a dipole field.

TABLE I

Open-flux fraction $f$ and polar-cap half-angle $\theta_c$ for $R_s/R = 2.5$

| $n$ | Source-surface model | | Current-sheet model | |
|---|---|---|---|---|
| | $f$ | $\theta_c$ (deg) | $f$ | $\theta_c$ (deg) |
| 1 | 0.581 | 49.7 | 0.506 | 45.4 |
| 3 | 0.675 | 41.0 | 0.586 | 36.7 |
| 5 | 0.711 | 35.6 | 0.616 | 31.5 |
| 7 | 0.730 | 31.9 | 0.631 | 28.0 |
| 9 | 0.741 | 29.1 | 0.640 | 25.5 |
| 11 | 0.748 | 27.0 | 0.647 | 23.5 |

Our next step is to inquire how sensitive this result is to the detailed form of the coronal model. For this purpose, we consider an alternate model in which the field is current-free everywhere except on the equatorial current sheet whose inner boundary occurs at $r = R_s$ (cf. Wolfson, 1985). The axisymmetric solution to Laplace's equation can then be written as

$$B_r(r, \theta) = \left(\frac{\Phi_0}{\pi R^2}\right) \sum_{l=1}^{\infty} [(l+1)\alpha_l (r/R)^{-l-2} - l\beta_l (r/R)^{l-1}] P_l(\cos\theta), \tag{7a}$$

$$B_\theta(r, \theta) = \left(\frac{\Phi_0}{\pi R^2}\right) \sum_{l=1}^{\infty} [\alpha_l (r/R)^{-l-2} + \beta_l (r/R)^{l-1}] P_l^1(\cos\theta), \tag{7b}$$

for $r < R_s$, and

$$B_r(r, \theta) = \pm\left(\frac{\Phi_0}{\pi R^2}\right) \sum_{l'=0}^{\infty} (l'+1)\gamma_{l'} (r/R_s)^{-l'-2} P_{l'}(\cos\theta), \tag{7c}$$

$$B_\theta(r, \theta) = \pm\left(\frac{\Phi_0}{\pi R^2}\right) \sum_{l'=0}^{\infty} \gamma_{l'} (r/R_s)^{-l'-2} P_{l'}^1(\cos\theta), \tag{7d}$$

for $r > R_s$. In Equations (7c) and (7d), the plus signs apply in the northern hemisphere ($0 < \theta < \pi/2$) and the minus signs apply in the southern hemisphere ($\pi/2 < \theta < \pi$). Also, the sums are restricted to terms with odd $l$ or even $l'$, depending on whether they refer to the field inside or outside $r = R_s$, respectively. As in the previous example, $\Phi_0$ refers to the total amount of photospheric flux of each polarity. Finally, in Equations (7b) and (7d), $P_l^1$ refers to the associated Legendre function of the first kind (Jahnke and Emde, 1945).

The coefficients $\alpha_l$, $\beta_l$, and $\gamma_l$ are determined from the boundary conditions as follows. First, matching $B_r(r, \theta)$ to the photospheric flux distribution given by Equation (2a), we obtain

$$(l+1)\alpha_l - l\beta_l = \left(\frac{n+1}{2}\right) a_l(n)\, \delta_{l \le n}\,, \tag{8a}$$

where $\delta_{l \le n} = 1$ if $l \le n$, and 0 otherwise. Second, by requiring both $B_r$ and $B_\theta$ to be continuous at $r = R_s$, we obtain the additional equations

$$\left(\frac{1}{2l+1}\right)[(l+1)\alpha_l \varepsilon^{l+2} - l\beta_l \varepsilon^{1-l}] =$$

$$= \sum_{l'=0}^{\infty} (l'+1)\, \gamma_{l'} \int_0^1 P_l(x) P_{l'}(x)\, \mathrm{d}x\,, \tag{8b}$$

$$\frac{l(l+1)}{(2l+1)}[\alpha_l \varepsilon^{l+2} + \beta_l \varepsilon^{1-l}] = \sum_{l'=0}^{\infty} \gamma_{l'} \int_0^1 P_l^1(x) P_{l'}^1(x)\, \mathrm{d}x\,, \tag{8c}$$

where $\varepsilon = R/R_s = 0.4$ as above. Third, as $r \to \infty$, $2\pi r^2 B_r$ must give the amount of open flux $f\Phi_0$ which means that $\gamma_0 = \varepsilon^2 f/2$, with the open-flux fraction $f$ again related to the polar-cap half-angle $\theta_c$ by Equation (5).

Eliminating $\alpha_l$ and $\beta_l$ from Equations (8), we obtain an infinite array of linear equations for the coefficients $\gamma_{l'}$:

$$\sum_{l'=0}^{\infty} (l'+1)\,[1 + l'\, d_l(R)] \int_0^1 P_l(x) P_{l'}(x)\, \mathrm{d}x\, \gamma_{l'} =$$

$$= c_l(R_s) \left(\frac{n+1}{2}\right) \int_0^1 x^n P_l(x)\, \mathrm{d}x\, \delta_{l \le n}\,, \tag{9}$$

where $l = 1, 3, 5, \ldots$ and $l' = 0, 2, 4, \ldots$; the coefficients $c_l(R_s)$ are given by Equation (3b), and the coefficients $d_l(R)$ are given by

$$d_l(R) = \frac{1 - \varepsilon^{2l+1}}{l + 1 + l\varepsilon^{2l+1}} \tag{10}$$

(cf. Nash, Sheeley, and Wang, 1988). In deriving this equation, we have used the identity $\int_0^1 P_l^1(x)P_{l'}^1(x)\,dx = l'(l'+1)\int_0^1 P_l(x)P_{l'}(x)\,dx$ for odd $l$ and even $l'$. Equations (9) are easily solved numerically using the algebraic expressions (6) for the accompanying integrals. Retaining terms through $l = 61$ and $l' = 60$, we evaluated $\gamma_0$ for odd values of $n$ from 1 to 11, and listed the corresponding values of $f$ and $\theta_c$ in columns 4 and 5 of Table I.

We find that the dipole field ($n = 1$) gives a polar-cap half-angle $\theta_c = 45.4°$ which is again much greater than the observed value of 30°. (By comparison, Wolfson (1985) obtained 45.9° by truncating the series at $l = 21$ and $l' = 20$.) Thus, the best fit is again obtained for $n > 1$, this time in the range 5–7, rather than 7–9 as found for the source-surface model. Also, the corresponding fraction of open flux is slightly less than obtained with the source-surface model, 62% compared to 74%.

Finally, as pointed out by Wolfson (1985), the MHD model of Pneuman and Kopp (1971) gives $f = 0.60$ and $\theta_c = 50.8°$ for the dipole field. These values are close to the values of $f = 0.58$ and $\theta_c = 49.7°$ obtained with the source-surface model, and well removed from the observed value of $\theta_c = 30°$. This suggests that even the MHD model would require a large value of $n$ to match the observed sizes of the polar coronal holes. Taken together, these three models indicate that the field is much more sharply peaked than a dipole distribution, and that approximately two-thirds of the photospheric flux resides in the 30° polar caps as footpoints of open field lines.

## 4. Magnetic Field Line Connections

In this section, we examine the magnetic field line connections that are produced between an evolving bipolar magnetic region and the nearby polar magnetic field, according to potential theory. For this purpose, we determine the coronal extension of the photospheric field using the source-surface method described in Section 3: We require that the radial component of the current-free coronal field match the photospheric flux distribution at $r = R$, and that the nonradial components vanish at the source surface located at $r = 2.5R$. By definition, open field lines are those which reach the source surface, and closed field lines are those which do not. We calculate the evolution of the photospheric flux distribution numerically using Leighton's (1964) transport equation, as modified by DeVore, Sheeley, and Boris (1984) to allow for a meridional surface flow (cf. Sheeley, DeVore, and Boris, 1985). The photosphere is represented by a computational grid consisting of 128 cells equally spaced in longitude and 64 cells equally spaced in latitude.

We begin with a reference calculation in which the polar field has the concentrated form $B = \pm 12\ \mathrm{G}\ |\cos\theta|^8$, where the minus (plus) sign applies in the northern (southern) hemisphere. Except for its sign, this field is the same as the one that Svalgaard, Duvall, and Scherrer (1978) deduced from observations around sunspot minimum in 1976. We introduce an idealized magnetic doublet whose leader pole of $-24 \times 10^{21}$ Mx lies at (29° N, 3° W) and whose follower pole of $+24 \times 10^{21}$ Mx lies at (32° N, 6° E) on May 21, 1987, as estimated for the large, new bipolar magnetic region in Figure 2. (These

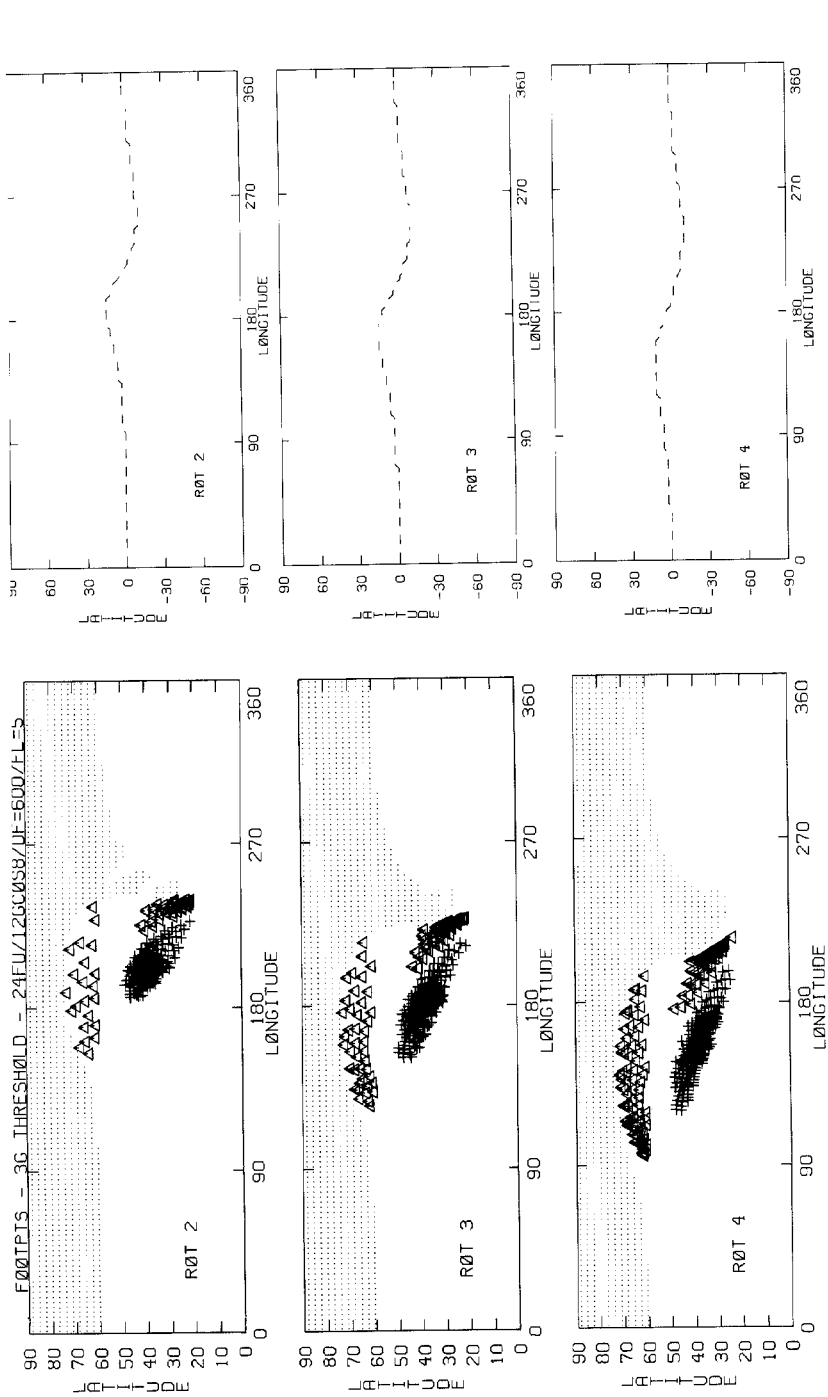


Fig. 2. *Left*: synoptic maps showing the northern-hemisphere footpoints of magnetic field lines at times that are two, three, and four Carrington rotations after the eruption of an idealized doublet source. *Right*: corresponding maps of the source-surface neutral line. *Dotted areas* show open-field regions; *triangles* show strong, negative-polarity fields which are connected to the doublet's positive pole; *plus signs* show strong, positive-polarity fields within the doublet which are connected either to its negative pole or to the north polar magnetic field. In this reference simulation, the doublet strength is $24 \times 10^{21}$ Mx, the background polar field is given by $B = +12\ \mathrm{G}\ |\cos\theta|^8$, and the threshold of strong field is 3 G. The regions of relatively strong closed field correspond to the regions of enhanced helium network in Figure 1, and the regions of open field correspond to helium coronal holes.

doublet fluxes are consistent with the measured values after correction for the poorly observed sunspot flux.) We let the resulting configuration evolve under the combined influences of supergranular diffusion at the rate $\kappa = 600$ km$^2$ s$^{-1}$, poleward meridional flow at the speed $v(\theta) = -5$ m s$^{-1}$ sin $2\theta$, and differential rotation at the Snodgrass (1983) rate $\omega(\theta) = 13.38 - 2.30 \cos^2 \theta - 1.62 \cos^4 \theta$ deg day$^{-1}$.

Figure 2 shows the results of this reference calculation at times that are two, three, and four 27.275-day Carrington rotations after the doublet source was deposited. The left panels show the northern-hemisphere locations of coronal holes and regions of strong, closed field which are not magnetically connected to the southern hemisphere. *Dotted areas* indicate open-field regions (i.e., coronal holes). *Triangles* indicate negative-polarity regions whose strengths exceed a nominal threshold level of 3 G and whose field lines extend to northern-hemisphere flux (i.e., to the positive pole of the doublet). Similarly, the *plus signs* indicate positive-polarity areas within the doublet, where the field strength exceeds 3 G and the field lines extend to northern-hemisphere flux (i.e., either to the negative pole of the doublet or to the north polar magnetic field). The density of the symbols plotted in these panels is determined by the fact that only one field line is traced for each of the 128 × 32 computational grid cells representing the northern hemisphere.

By elimination, the blank spaces on these maps represent closed-field regions where the field either is less than 3 G, or is greater than 3 G and is connected to southern-hemisphere flux. (We note for completeness that some blank spaces occur between the high-latitude *triangles* and the polar coronal hole, indicating the presence of a narrow transition region of negative field in excess of 3 G that is connected by very long field lines to positive flux in the southern hemisphere.) In the right panels, the *dashes* show the corresponding equatorial source-surface neutral lines. In all of these maps, the longitude scale has been shifted by 90° so that the region of interest is centered near 180°, rather than between 270° and 360° as observed for the associated helium structures in Figure 1.

The left panels of Figure 2 show several features in common with the helium images. First, at longitudes well removed from the bipolar region, the polar-hole boundary lies at 60° latitude, and does not change with time. To prevent the hole boundary from moving poleward, it was necessary to choose meridional flow rates that reduced to relatively low values at high latitude. Although we adopted a speed of 5 m s$^{-1}$ peaked at 45° latitude in our reference calculation, we also found that a 10 m s$^{-1}$ flow peaked at 30° latitude gave essentially the same result.

Second, a small coronal hole forms in the negative flux at the leading end of the bipolar region and gradually merges with the equatorward-moving lobe of the polar hole during rotations 2–4. During this time, the polar-hole lobe drifts eastward with the enhanced field in the bipolar region, and remains relatively unsheared by differential rotation. Its synodic rotation period is approximately 28.5 days, corresponding to a latitude of 32° at the Snodgrass (1983) rate.

Third, in the latitude range 60–75°, a band of enhanced field has become connected to the positive pole of the bipolar region. This reconnected field lies in the region where

the polar-hole boundary has receded northward and where the enhanced helium network is visible in Figure 1. It is separated from the strong field in the bipolar region by a latitude gap of about 7°, which is comparable to the 10° separation of the corresponding helium features in Figure 1. Despite its relatively high latitude, the reconnected field drifts eastward at approximately the same rate as the bipolar flux in the 30–40° range, and suffers a comparable elongation in longitude. Its synodic rotation period is approximately 29 days, corresponding to a latitude of 36°.

The right panels of Figure 2 show the corresponding distortion of the source-surface neutral line. Its northward and southward excursions occur at approximately the longitudes of the receded and expanded parts of the polar-hole boundary, respectively, and its eastward drift rate is likewise comparable to that of the photospheric flux in the bipolar region. This is a simple illustration of the fact that the source-surface field rotates quasi-rigidly at a rate corresponding to the latitude of the unwound, nonaxisymmetric photospheric flux (Wang *et al.*, 1988), which in this case resides in the evolving bipolar region.

Also, because the footpoints of the open-field lines tend to corotate with their source-surface extensions (Nash, Sheeley, and Wang, 1988), this explains why the simulated polar-hole lobe rotates without distortion at approximately the rate of the bipolar region and why the simulated polar-hole intrusion also rotates at this rate rather than with the 35-day period corresponding to its latitude of 60–75°. Of course, this explanation also accounts for the observed behavior of the corresponding helium features, whose rotational properties are reproduced in our simulations. In particular, we can now understand why the recurrence patterns of coronal holes and their associated interplanetary sectors changed from 27-day patterns to 28.5-day patterns in mid-1977 (Sheeley and Harvey, 1981) and again in mid-1987 during the rising phase of the present sunspot cycle 22.

In Figure 3, we show that by reducing the polar field strength from 12 G to 6 G, we obtain a greater deformation of the polar-hole boundary and its associated source-surface neutral line. The reconnected field intrudes 5° farther into the polar hole and the polar-hole lobe extends about 2° closer to the equator. Also, the corresponding warps in the source-surface neutral line now extend about 21° farther to the north and 4° farther to the south, respectively. The band of reconnected field is narrower than the one obtained in Figure 2, and it is separated from the enhanced field in the bipolar region by the greater distance of 13°. However, as illustrated in Figure 5 below, the latter differences reflect our choice of enhancement threshold, whose 3 G value is somewhat larger than required to match the observed width and separation of the helium features. Finally, we note that by the fourth rotation, the negative-polarity coronal hole in the leading part of the bipolar region is now accompanied by a small, positive-polarity hole in the trailing part. For a sufficiently weak polar field, we would expect coronal holes to form in both parts of the bipolar region as some of its closed field lines reach the source surface and become open.

In a calculation not shown here, we found that reducing the polar field strength to 3 G caused the band of reconnected field to extend still further poleward to N 85°, in

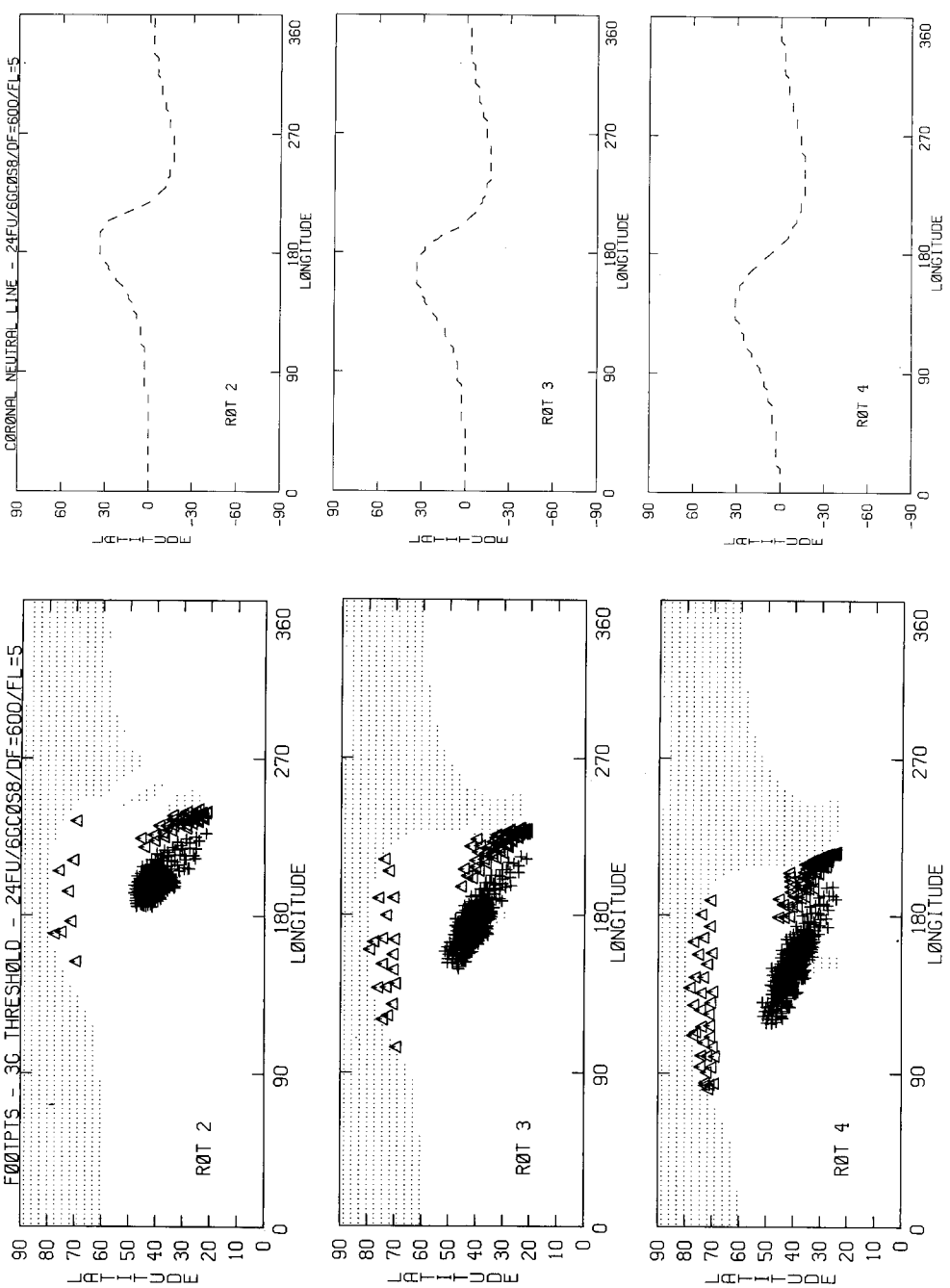


Fig. 3. The same as Figure 2, except that the polar field strength has been reduced to 6 G. By weakening the polar field, we increase the deformation of the polar-hole boundary and its associated source-surface neutral line, and we produce a small positive-polarity coronal hole in the trailing end of the bipolar region.

even greater disagreement with the helium observations. Thus, for a doublet flux of $24 \times 10^{21}$ Mx, the best agreement with the helium observations is obtained with a polar field strength of about 12 G. However, as discussed in the next section, the derived strength of the polar field depends on the assumed distribution of flux at high latitude, and for a flat distribution the polar field strength may be as small as 6 G.

In Figure 4, we show that the amounts of deformation and warping are reduced when the polar field strength is returned to 12 G and the doublet flux is decreased from $24 \times 10^{21}$ Mx to $12 \times 10^{21}$ Mx. Now, the extension of the polar-hole lobe, the intrusion

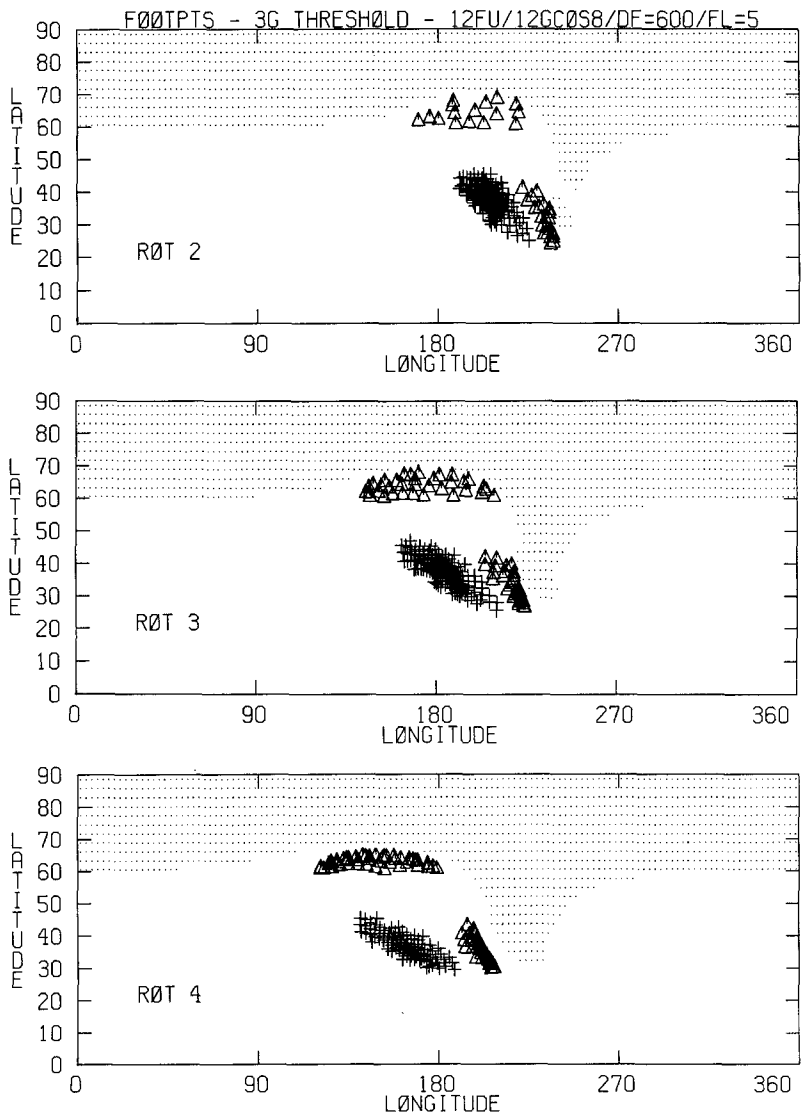


Fig. 4. The same as Figure 2, except that the doublet strength has been reduced to $12 \times 10^{21}$ Mx and the source-surface neutral line is not shown. By weakening the source, we decrease the deformation of the polar-hole boundary and the source-surface neutral line.

of the high-latitude enhancement, and the warping of the source-surface neutral line (not shown here) are all less than obtained with the reference conditions of Figure 2. Also, the enhanced regions of closed field are smaller and the gap separating them is a few degrees wider than obtained for the reference conditions. However, these latter differences again reflect our choice of a 3 G enhancement threshold, and are smaller when the threshold is reduced to 2 G.

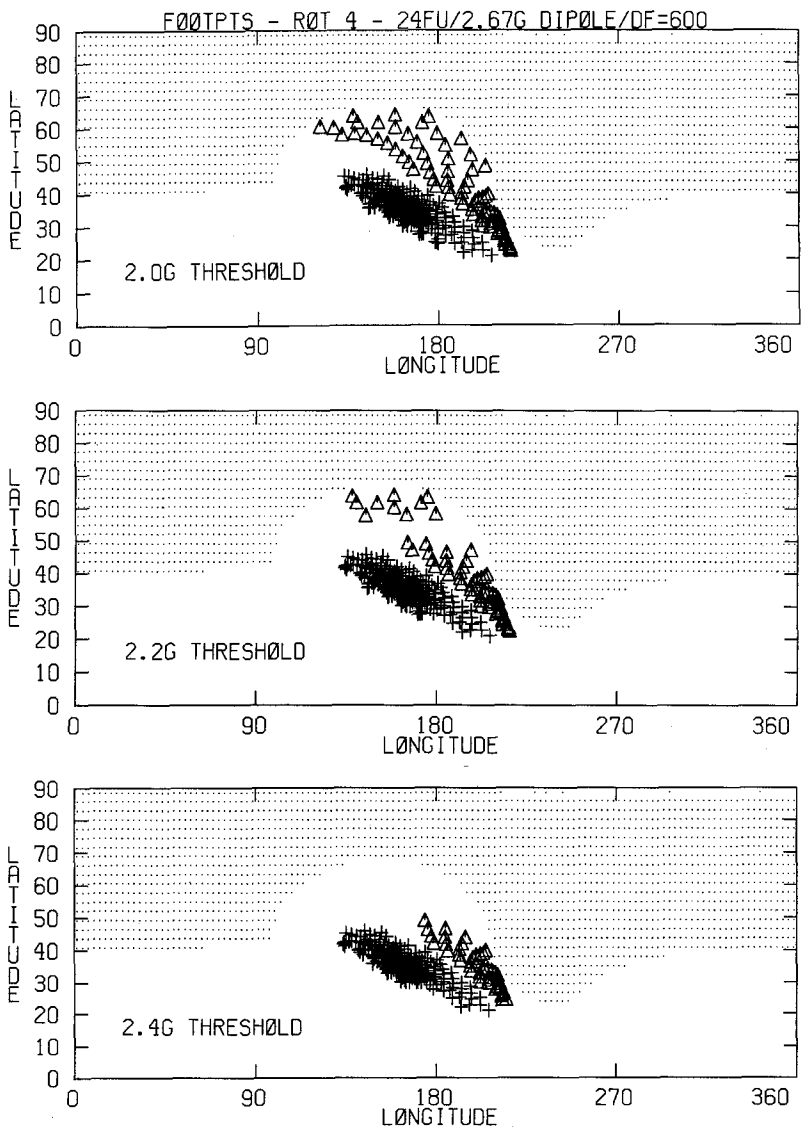


Fig. 5. Synoptic maps of the northern-hemisphere footpoints at the same time (the fourth rotation), but with different values of the field-strength enhancement threshold (2.0, 2.2, and 2.4 G). In this case, the doublet strength is again $24 \times 10^{21}$ Mx, but the polar flux is distributed more widely in latitude according to the dipole expression $B = 2.67$ G $\cos\theta$. None of these maps provides satisfactory agreement with the helium observations, suggesting that the Sun's polar field is more concentrated than a dipole field.

The effect of varying the enhancement threshold is shown in Figure 5 for a polar field of the form $B = 2.67$ G $\cos\theta$. This dipole field contains the same amount of flux as the $B = \pm 12$ G $|\cos\theta|^8$ distribution. Also, in this case, we return the doublet to its original strength of $24 \times 10^{21}$ Mx, and remove meridional flow, which would rapidly reconcentrate the polar flux. Unlike the previous figures which indicate field-line connections at different times, this figure shows the connections at the same time (the fourth rotation), but with different choices of enhancement threshold (2.0, 2.2, and 2.4 G).

None of the maps in Figure 5 provides a satisfactory agreement with the helium observations. The relatively low enhancement threshold of 2.0 G causes the gap between the high-latitude reconnections and the bipolar region to become filled in, and the high threshold of 2.4 G exceeds the strength of all of the reconnected fields at high latitude. Only the 2.2 G threshold provides a gap, but its 3° width is significantly smaller than the 10° gap observed in the helium images. Although the polar hole recedes as far north as 70° latitude, relatively little of this recessed area consists of reconnected fields whose strengths exceed the 2.2 G threshold, the longitudinal extension of these fields being about 45° less than obtained with the reference conditions. Finally, perhaps the greatest discrepancy occurs at longitudes well removed from the eruption, where the polar-hole boundary lies at 40° latitude rather than at the observed latitude of 60° (cf. Table I). Clearly, the observations require a concentrated polar magnetic field.

## 5. Discussion

The overall agreement between the calculated field-line connections in Figure 2 and the observed modulations of the helium network in Figure 1 suggests an interpretation in terms of the field-line topology. We suppose that as the field lines of the new bipolar region expand into the corona, they encounter and reconnect with field lines of the Sun's polar magnetic fields. In this way, some of the bipolar region's positive flux becomes connected to negative flux at high latitude, thereby producing an intrusion in the polar coronal hole and a northward deflection of the neutral sheet in the outer corona. Some of the corresponding disconnected field lines from the bipolar region's negative pole remain open, as shown by the small coronal hole in the first panel of Figure 2. However, others reconnect with relatively long, closed field lines that extend into the southern hemisphere. In this way, open flux shifts westward from the high-latitude intrusion to the lower-latitude lobe of the polar coronal hole where it produces a shouthward deflection of the outer-coronal neutral sheet. Thus, some of the bipolar region's negative flux becomes open, some becomes connected to positive flux in the southern hemisphere, and some remains connected to the positive flux with which it erupted.

We can interpret the helium enhancements (darkenings) in terms of the heating that is responsible for the associated patterns of X-ray and XUV coronal emission. According to Sturrock and Uchida (1981) and Parker (1983), the heating is produced by the dissipation of small-scale distortions induced in the field lines by photospheric motions of their footpoints. In these models, the heating rate depends on the length of a loop as well as the strength of the field in which it is anchored, with the greatest heating being

obtained for short loops anchored in strong fields. This is consistent with our finding that the patterns of enhanced helium network occur in the new bipolar region and in the strong-field region to which it becomes connected at the edge of the nearby polar cap. Evidently, in these examples the field-line connections to the opposite hemisphere were too long to produce appreciable heating because helium enhancements did not occur there.

It is significant that we need a concentrated polar field in order to interpret the enhancements and weakenings of the helium network in terms of magnetic field line connections. Not only does this provide support for the analysis of Svalgaard, Duvall, and Scherrer (1978) who found a concentrated polar field, but also it adds to the growing list of evidence for the presence of a poleward meridional flow. In their analytical calculations, DeVore, Sheeley, and Boris (1984) showed that a poleward meridional flow is necessary to concentrate the field. In simulations of the Sun's photospheric rotation, it was necessary to supplement supergranular diffusion with a $10\ \mathrm{ms}^{-1}$ poleward flow in order to match the rotation rate and equatorial correlation size of the observed field (Sheeley, Nash, and Wang, 1987). In simulations of the rotation of the coronal magnetic field, this poleward flow was required in order to match the curvature and asymmetry of the observed rotation profiles during the rising phase of the sunspot cycle and the 28-day recurrence period near sunspot maximum (Wang *et al.*, 1988).

It is important to recognize that the derived polar magnetic field strengths depend on the assumed distribution of flux at high latitude. For a highly peaked distribution of the form $B = \pm B_0 |\cos \theta|^8$, we were able to fit the observations best with $B_0 = 12$ G. However, in calculations not shown here, we have also been able to match the observations using a field that has a uniform strength of 6 G within 35° of the poles and which falls to negligible values at lower latitudes. This field contains approximately the same amount of flux as the stronger, more highly peaked field. As in the previous section, we found that a uniform polar-cap field of only a few Gauss caused the coronal-hole boundary to recede much more than is shown by the helium observations.

The essential point is that the distortion of the polar-hole boundary depends on the relative amounts of flux in the perturbing bipolar region and in the polar cap. Thus, for an observed distortion, the easily measured flux in the bipolar region determines the amount of flux that must lie at high latitudes where accurate measurements are difficult. The fact that most of this flux must reside within about 30–35° of the poles, in turn, places a constraint on the average polar-cap field strength, which we have seen is about 6 G. At lower latitudes, the rapid falloff of field strength gives rise to the observed gap between the strong-field enhancements in the bipolar region and at the edge of the nearby polar coronal hole.

Finally, we emphasize that the deformation of the polar-hole boundary and its source-surface neutral line occurs on the time-scale for the flux to erupt in the bipolar region. We expect such rapid deformations to be accompanied by sudden fluctuations in the rotation rate of the outer-coronal field, provided that the newly erupting flux is large and occurs out of phase with the nonaxisymmetric component of the background field. (Of course, in this paper the background field was purely axisymmetric and its

rotation rate was therefore undefined.) By contrast, the subsequent symmetrization is a much slower process that occurs gradually over several solar rotation periods, as differential rotation and supergranular diffusion combine to wipe out the Sun's nonaxisymmetric flux (Sheeley and DeVore, 1986; DeVore, 1987; Wang *et al.*, 1988). Thus, we would expect the distortion of the coronal streamer belt during the rising phase of the sunspot cycle to be a much more rapid process than its smoothing out during the declining phase of the cycle.

## Acknowledgements

We gratefully acknowledge the help of our colleague Ana G. Nash during the initial phase of this work. We also thank our colleagues Spiro T. Antiochos and John. T. Mariska for useful conversations about coronal heating. Financial and other support was provided in part by the Solar Physics Branch of the NASA Space Physics Division (DPR W-14429) and by the Office of Naval Research.

## References

Altschuler, M. D. and Newkirk, G.: 1969, *Solar Phys.* **9**, 131.
Bohlin, J. D.: 1977, *Solar Phys.* **51**, 377.
Bohlin, J. D. and Rubenstein, D. M.: 1975, World Data Center A Report UAG-51.
Bohlin, J. D. and Sheeley, N. R., Jr.: 1978, *Solar Phys.* **56**, 125.
Broussard, R. M., Sheeley, N. R., Jr., Tousey, R., and Underwood, J. H.: 1978, *Solar Phys.* **56**, 161.
Chapman, G. A.: 1972, *Solar Phys.* **24**, 288.
D'Azambuja, L. and D'Azambuja, M.: 1938, *Bull. Astron.* **11**, 349.
DeVore, C. R.: 1987, *Solar Phys.* **112**, 17.
DeVore, C. R., Sheeley, N. R., Jr., and Boris, J. P.: 1984, *Solar Phys.* **92**, 1.
Giovanelli, R. G., Hall, D. N. B., and Harvey, J. W.: 1972, *Solar Phys.* **22**, 53.
Harvey, J. W. and Hall, D.: 1971, in R. Howard (ed.), 'Solar Magnetic Fields', *IAU Symp.* **43**, 279.
Harvey, J. W., Krieger, A. S., Timothy, A. F., and Vaiana, G. S.: 1975, *Osserv. Mem. Oss. Astrofis. Arcetri* **104**, 50.
Harvey, J. W. and Sheeley, N. R., Jr.: 1977, *Solar Phys.* **54**, 343.
Harvey, J. W. and Sheeley, N. R., Jr.: 1979, *Space Sci. Rev.* **23**, 139.
Harvey, K. L.: 1984, *Proc. 4th European Meeting on Solar Physics*, Noordwijkerhout, The Netherlands, October 1–3, 1984, ESA SP-220, p. 235.
Harvey, K. L.: 1985, *Australian J. Physics* **38**, 875.
Harvey, K. L., Sheeley, N. R., Jr., and Harvey, J. W.: 1980, *Bull. Am. Astron. Soc.* **12**, 503.
Harvey, K. L., Sheeley, N. R., Jr., and Harvey, J. W.: 1986, in P. A. Simon, G. Heckman, and M. A. Shea (eds.), *Solar-Terrestrial Predictions: Proceedings of a Workshop at Meudon, France, June 18–22, 1984*, published by NOAA/AFGL, p. 198.
Hoeksema, J. T.: 1984, 'Structure and Evolution of Large Scale Solar and Heliospheric Magnetic Fields', Ph.D. Thesis, Stanford University.
Jahnke, E. and Emde, F.: 1945, *Tables of Functions*, Dover, New York, p. 110.
Leighton, R. B.: 1964, *Astrophys. J.* **140**, 1547.
Nash, A. G., Sheeley, N. R., Jr., and Wang, Y.-M.: 1988, *Solar Phys.* **117**, 359.
Parker, E. N.: 1983, *Astrophys. J.* **264**, 642.
Pneuman, G. W. and Kopp, R. A.: 1971, *Solar Phys.* **18**, 258.
Schatten, K. H., Wilcox, J. M., and Ness, N. F.: 1969, *Solar Phys.* **6**, 442.
Sheeley, N. R., Jr.: 1980, *Solar Phys.* **65**, 229.
Sheeley, N. R., Jr. and DeVore, C. R.: 1986, *Solar Phys.* **103**, 203.

Sheeley, N. R., Jr. and Harvey, J. W.: 1978, *Solar Phys.* **59**, 159.
Sheeley, N. R., Jr. and Harvey, J. W.: 1981, *Solar Phys.* **70**, 237.
Sheeley, N. R., Jr., DeVore, C. R., and Boris, J. P.: 1985, *Solar Phys.* **98**, 219.
Sheeley, N. R., Jr., Nash, A. G., and Wang, Y.-M.: 1987, *Astrophys. J.* **319**, 481.
Snodgrass, H. B.: 1983, *Astrophys. J.* **270**, 288.
Sturrock, P. A. and Uchida, Y.: 1981, *Astrophys. J.* **246**, 331.
Svalgaard, L., Duvall, T. L., and Scherrer, P. H.: 1978, *Solar Phys.* **58**, 225.
Tousey, R.: 1967, *Astrophys. J.* **149**, 239.
Tousey, R.: 1971, *Phil. Trans. Roy. Soc. London* **A270**, 59.
Tousey, R., Bartoe, J. D. F., Bohlin, J. D., Brueckner, G. E., Purcell, J. D., Scherrer, V. E., Sheeley, N. R., Jr., Schumacher, R. J., and Van Hoosier, M. E.: 1973, *Solar Phys.* **33**, 265.
Wang, Y.-M., Sheeley, N. R., Jr., Nash, A. G., and Shampine, L. R.: 1988, *Astrophys. J.* **327**, 427.
Wolfson, R.: 1985, *Astrophys. J.* **288**, 769.
Zirin, H. and Howard, R.: 1966, *Astrophys. J.* **146**, 367.